Deborah J. Rubens, MD • Mark A. Hadley, MD, PhD • Sheik Kaisar Alam, MS • Lan Gao, MS
Robert D. Mayer, MD • Kevin J. Parker, PhD

Sonoelasticity Imaging of Prostate Cancer: In Vitro Results[1]

PURPOSE: **To compare sonoelasticity imaging versus ultrasound (US) in detection of prostate cancer.**

MATERIALS AND METHODS: **Sonoelasticity imaging and US were performed on 10 prostatectomy specimens in which cancer was detected at previous biopsy. Six patients had no palpable lesions at digital rectal examination. Specimens were imaged axially at the apex, middle, and base of the gland to correlate with location of pathologic sections. All images were interpreted blindly and prospectively, and results were compared with pathologic findings.**

RESULTS: **Sensitivity and specificity with sonoelasticity imaging were 85% and 84%, respectively, and 30% and 100% with standard US when compared with pathologic findings. Sixty-four percent of pathologically confirmed tumors detected at sonoelasticity imaging were isoechoic on conventional US images.**

CONCLUSION: **In this limited study, sonoelasticity imaging was more sensitive for tumor detection and more accurate for assessment of tumor location than was conventional US.**

Index terms: Prostate, neoplasms, 844.32 • Prostate, US, 844.1298 • Ultrasound (US), experimental, 844.12984

Radiology 1995; 195:379–383

SONOELASTICITY imaging was initially developed by Lerner et al (1) to detect the relative stiffness of tissues on the basis of differential vibration characteristics. With sonoelasticity imaging, tissue is vibrated with a low-frequency source and tissue motion is detected and displayed as a color image superimposed on the conventional gray-scale ultrasound (US) image. Results of early studies in phantom and animal models confirmed that isoechoic lesions on gray-scale images could be differentiated with sonoelasticity imaging because of their differing sensitivity to vibration (1). The theory of sonoelasticity imaging is based on the postulate that low-frequency vibrations are easily conducted through soft tissue and muscle; discrete stiff tumors, however, create a detectable disturbance in the vibration pattern. This theory was successfully applied to canine and human prostatectomy specimens with modified laboratory equipment (2). These early investigations demonstrated a clear correlation between vibration image deficits and areas of palpable stiffness. The current study was performed with specially modified, commercially available equipment to test the hypothesis that sonoelasticity imaging in vitro could enable detection of nonpalpable prostate cancer that appears normal at US.

MATERIALS AND METHODS

Ten specimens obtained at radical prostatectomy from patients with biopsy-proved adenocarcinoma were scanned with standard US and sonoelasticity imaging immediately after surgery. Preoperative diagnosis of carcinoma was made on the basis of histologic findings at transrectal US–guided biopsy in nine patients and transurethral prostatectomy in one. Transrectal US was performed by a urologist (R.D.M.), and findings were correlated with those obtained at digital rectal examination and with prostatic-specific antigen (PSA) levels (Table 1). Biopsy specimens were obtained from six palpable hypoechoic lesions and random sextant biopsy specimens from three patients with normal transrectal US findings. Preoperative transrectal US findings and biopsy results were not available at the time of specimen scanning or image interpretation.

After prostatectomy, specimens were transported on ice and were scanned within 30 minutes of removal from the body. Specimens were placed prone in a clear plastic container lined with plastic wrap. The container was open like a doughnut inferiorly to allow direct contact between the specimen and the vibration source anteriorly (Fig 1). Specimens were stabilized within a cutout gel standoff pad and surrounded with US gel for acoustic coupling.

Imaging was performed with a 7-MHz linear-array transducer clamped in position with a thin layer of gel on the perirectal surface so as not to dampen the acoustic vibration originating from the opposite side. US and sonoelasticity imaging locations were chosen by visually dividing the specimen into thirds and imaging in the axial plane, perpendicular to the gland, at the base, midportion, and apex; in addition, some lesions were confirmed in the longitudinal plane. Distance between images depended on gland size and was not controlled by an external stepping apparatus. Section thickness was dictated by the transducer face and the elevation plane thickness of the ultrasound beam at the focal zone. Images were recorded on laser film, color transparency, or paper. All imaging was performed with a commercially available instrument (Acuson 128XP; Acuson, Mountain View, Calif).

Tissue vibration was accomplished by shear wave production from a cone-shaped source that lightly touched the dependent surface of the prostate. Vibration frequencies that were sampled ranged from 50 to 250 Hz, with a peak source amplitude of less than 0.1 mm. Specially modified proprietary software was used to display vibration within tissue as a "green-tag" overlay on the image. That is, Doppler receiver parameters were set to a

Abbreviation: PSA = prostate-specific antigen.

[1] From the Departments of Diagnostic Radiology (D.J.R., M.A.H.), Electrical Engineering (S.K.A., L.G.), and Urology (R.D.M., K.J.P.), University of Rochester School of Medicine and Dentistry, 601 Elmwood Ave, Rochester, NY 14642-8648. From the 1993 RSNA scientific assembly. Received August 22, 1994; revision requested September 26; revision received December 29; accepted January 3, 1995. Address reprint requests to D.J.R.

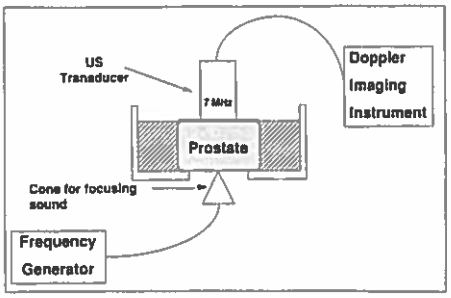

Figure 1. Diagram of sonoelasticity imaging apparatus. Prostate gland is surrounded by acoustic coupling gel (black area) and stabilized by a cut-out gel pad (stippled area). A 7-MHz linear-array transducer on a specially modified computed sonography unit was used to image the prostate in gray-scale and vibration (Doppler) modes.

green-tag function, which is based on an estimate of the standard deviation of the Doppler spectrum. Normal vibrating tissue above a threshold of approximately 0.02-mm displacement was identified as green, and nonvibrating tissue as gray-scale image. The current software version displays the green-tag function as an all-or-none function, without shading, to represent amplitude of vibration above a threshold. Areas of no gray-scale image (ie, shadows) also do not display a green-tag vibration image.

After imaging, specimens were transported on ice to the pathology department for sectioning. Glands were sectioned per routine protocol in 4-mm slices from apex to base. Each slice was divided into quarters, which were labeled left anterior, right anterior, left posterior, and right posterior; in addition, each slice was lettered alphabetically and subnumbered from apex to base (eg, apex = a_1 and a_2). Depending on the length of the prostate, as few as four or as many as 10 slices may be required. A single slide was prepared from the surface of each slab in each cassette. Pathologic results were obtained from departmental dictated reports and review of original sections in questionable areas. Tumor location and extent were recorded by a pathologist; tumor size and volume, however, were not. In addition, because pathologic sectioning followed US imaging, no direct correlation between precise tumor boundaries could be obtained.

US and sonoelasticity images were reviewed off-line and visually divided into anterior and posterior and right and left segments to best correspond to the pathologic cassettes. Because preoperative transrectal US was performed for biopsy only and imaging results were not recorded for each segment at each level, they could not be directly correlated with in vitro sonoelasticity and US images.

US images were scored as positive for tumor when a discrete hypoechoic nodule or region was identified (3–5). Sonoelasticity images were scored as positive for tumor when a normally visualized gray-scale image did not fill in uniformly with the green-tag vibration signal. Sonoelasticity imaging defects could be focal (well circumscribed with no vibration) or diffuse (poorly marginated with green pixels [vibration] incompletely filling in the gray-scale image). Scoring of US and sonoelasticity images was performed blindly and prospectively (reader 1, D.J.R.) without knowledge of initial transrectal US, digital rectal examination, or pathologic reports and findings; a second blinded interpretation of sonoelasticity images was also performed (reader 2, K.J.P.). Separate statistical analyses were performed and a κ statistic obtained (6) to analyze interobserver variation. Pathologic reports and sections were reviewed (by M.A.H.) without knowledge of transrectal US, US, or sonoelasticity imaging results and scored for tumor presence or absence. At the time of composite review, 108 sonoelasticity images and US quadrant images were available to all reviewers and form the data base for this study. US and sonoelasticity images were compared with pathologic findings for each section and each patient.

Table 1
Preoperative Diagnosis of Prostate Cancer

Patient	PSA Level* (ng/mL)	Findings at Digital Rectal Examination	Findings at Transrectal US	Findings at US of Specimen
1	9.4	Nodule, midline, mid-gland to apex	Hypoechoic at site of digital rectal examination finding	Hypoechoic, midline apex to base
2	4.3	Nodule, left base of gland	Hypoechoic at site of digital rectal examination finding	Normal
3	13.4	Nodule, left midgland	Hypoechoic bilaterally	Hypoechoic, right side
4	9.8	Normal	Normal	Hypoechoic, right base to apex and left midgland peripheral zone
5	4.2	Indurated right lobe	Hypoechoic right lobe	Normal
6	2.5	Normal	Transurethral US not performed; A_2 carcinoma noted at examination of transurethral prostatectomy	Hypoechoic apex, anterior
7	12.2	Normal	Normal	Abnormal, right peripheral gland base to apex
8	8.9	Nodule, left midgland	Abnormal peripheral zone at abnormal digital rectal examination site	Hypoechoic, right and left base to apex peripheral zone
9	6.7	Nodule, left midgland	Abnormal peripheral zone at abnormal digital rectal examination site	Normal
10	10.1	Normal	Normal	Abnormal, left and right base posteriorly

* Monoclonal assay; normal = ≤4 ng/mL.

Table 2
Results of Sonoelasticity Imaging and US versus Examination of Pathologic Specimens

Result	Sonoelasticity Imaging			US
	Reader 1	Reader 2	Mean	
True positive (*n*)	66	70	68.0	24
True negative (*n*)	26	21	23.5	28
False positive (*n*)	2	7	4.5	0
False negative (*n*)	14	10	12.0	56
Sensitivity (TP[TP + FN])*	0.83	0.88	0.85	0.30
Specificity (TN[TN + FP])†	0.93	0.75	0.84	1.0
Positive predictive value (TP[TP + FP])	0.97	0.91	0.94	1.0
Negative predictive value (TN[TN + FN])	0.65	0.68	0.66	0.33
Accuracy (TP + TN)/(TP + TN + FP + FN)	0.85	0.84	0.85	0.48

Note.—FN = false negative, FP = false positive, TN = true negative, TP = true positive.
* $P < .0001$ (Fisher Exact Test), extremely significant.
† $P = .115$ (Fisher Exact Test), not significant.

RESULTS

In this preselected population, sonoelasticity imaging yielded an 85% sensitivity and 84% specificity for car-

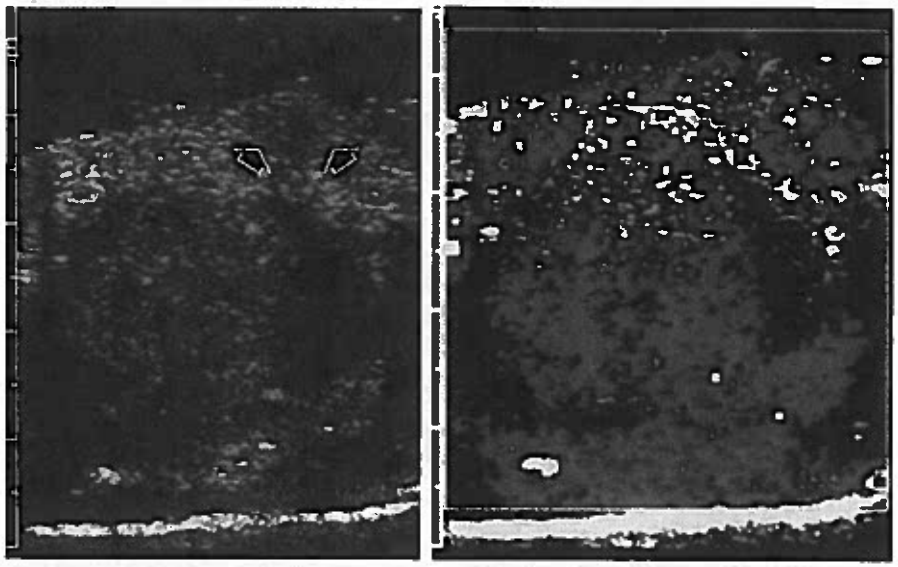

a. b.

Figure 2. Focal nodule of prostate carcinoma at (a) standard US and (b) sonoelasticity imaging in a 60-year-old man with a serum monoclonal PSA level of 13.4 ng/mL and a palpable nodule at the left apex of the prostate. (a) Left sagittal standard US image shows a discrete hypoechoic mass in the posterior apex (arrows) that corresponds to findings at clinical examination. (b) At sonoelasticity imaging, this area did not vibrate at the same amplitude as the surrounding prostate tissue (green areas) and, therefore, is displayed as an area of color void. A second, more central nonvibrating region beneath the peripheral nodule is seen at sonoelasticity imaging but not at US. Both defects identified at sonoelasticity imaging corresponded to foci of carcinoma in the prostate specimen.

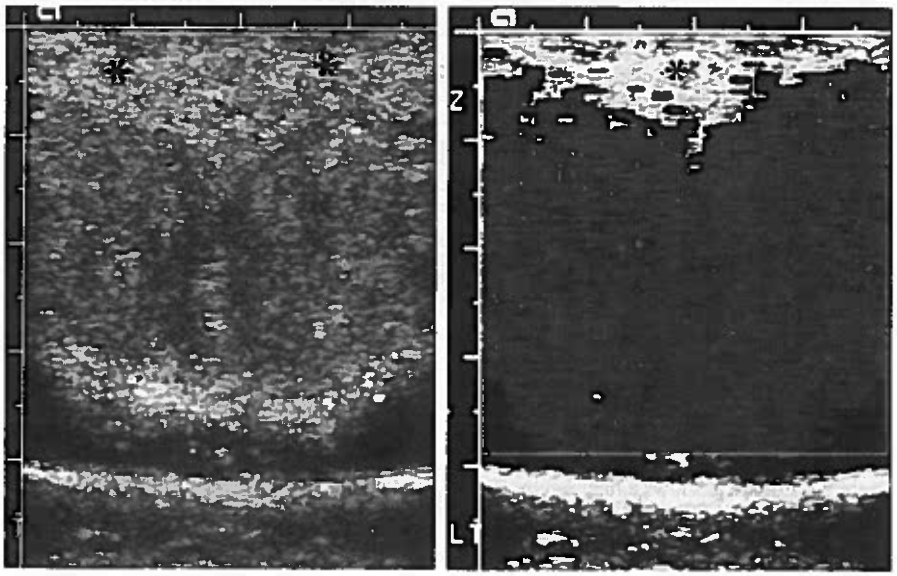

a. b.

Figure 3. Isoechoic carcinoma depicted on sonoelasticity image of a 67-year-old man with no discrete palpable lesion and a serum PSA level of 4.2 ng/mL. (a) Standard prone transverse US image obtained at the apex demonstrates normal peripheral zone tissue bilaterally (*). (b) Sonoelasticity image shows a triangular region of absent vibration (*), which at histologic examination proved to be carcinoma.

cinoma in prostate segments (combined results of both readers)(Table 2). Standard in vitro US was 30% sensitive and 100% specific for prostate cancer (Table 2). Eighty of 108 segments contained carcinoma. All disease was bilateral and involved at least four segments (mean, eight segments). No tumor-containing segment was detected at US that was not also detected at sonoelasticity imaging. Most important, 44 of 68 tumor-containing segments detected at sonoelasticity imaging were not identified at conventional US.

The pathologic review of seven segments found to be false-positive at sonolastic imaging by both readers yielded prostatic intraepithelial neoplasia in one segment, stromal and glandular hyperplastic nodules 8–10 mm in diameter in two, and diffuse stromal hyperplasia in four. Diffuse, nonnodular glandular hyperplasia was noted in review of some true-negative segments.

Sonoelasticity images demonstrated focal nonvibrating nodules that correlated with those on standard gray-scale images (Fig 2) and also showed diffuse infiltrative tumor not depicted on gray-scale images (Fig 3). Although the vibration source was located on the anterior surface opposite the receiving transducer, both anterior and posterior tumor-containing segments were identified. Reader 1 correctly identified 18 anterior tumor segments on sonoelasticity images, compared with 22 identified by reader 2. Both readers correctly identified tumor in 48 posterior segments. Sonoelasticity imaging defects were observed through a broad range of frequencies, from 50 to 240 Hz (Fig 4). Both readers agreed overall on findings in 88 of 108 sections. The κ statistic, calculated according to the method of Fleiss (6), was .56.

For each patient, and on the presumption that US abnormalities would direct biopsy, three of 10 specimens had no gray-scale findings for tumor, for a sensitivity of 70% for standard US. Preoperatively, abnormalities in these same three specimens at transrectal US correlated with those at digital rectal examination. Conversely, three patients with normal findings reported preoperatively at transrectal US had focal hypoechoic peripheral zone lesions at pospoperative US of the specimen (Table 1). At sonoelasticity imaging, tumor was detectable in some portion of all specimens, for 100% sensitivity in each patient.

DISCUSSION

Sonoelasticity imaging offers a unique advantage over transrectal US and digital rectal examination because it combines and extends in a single examination features of both procedures. In addition to posterior and apical lesions, sonoelasticity imaging enables detection of characteristic tumor stiffness in anterior, lateral, and superior regions of the prostate that are inaccessible at digital rectal examination. An isoechoic tumor noted at transrectal US may be detected because of its different vibration pattern. The standard features of transrectal US diagnosis are maintained, includ-

ing the ability to measure prostate volume to correlate with PSA levels and identification of discrete hypoechoic lesions and areas of asymmetry or capsular distortion to direct biopsy.

Sixty-five percent of tumor-containing segments detected at sonoelastic imaging were not identified at US; thus, sonoelasticity imaging offers substantial potential to improve prostate cancer detection and staging. Given the experience reported in the radiology and urology literature, these results are not surprising: Only 32%–42% of prostate carcinomas in each lobe were detectable at standard US (7,8). Even when directed and random biopsy procedures were performed (8), the number of prostate cancers undetected at transrectal US is substantial. In the series of 134 cancerous prostate lobes reported by Slonim et al (8), 78 (58%) demonstrated no hypoechoic lesion at standard transrectal US, and findings in 43 (32%) were false-negative when biopsy and prostatectomy results were compared. In the series of 153 patients reported by Daniels et al (9), carcinoma was detected in 37 (24%) sonographically and palpably normal prostate lobes when the contralateral lobe contained carcinoma. A method such as sonoelasticity imaging potentially could improve the false-negative biopsy rate by demonstration of vibration abnormalities in areas that appear normal at sonography. Inasmuch as US-guided biopsy may some day be used for triage and staging, segmental imaging that permits identification of bilateral disease and estimatation of disease extent may be important in patient care.

Sensitivity of sonoelasticity imaging for tumor diagnosis was markedly improved over that of in vitro US ($P < .0001$, extremely significant). This is due in part to low gray-scale sensitivity to tumor in individual segments, which made sensitivity of sonoelasticity imaging in our study more striking. Another limitation of in vitro imaging is distortion of normal anatomic relationships, which makes it difficult to detect tumor on the basis of gland asymmetry or capsular bulging. This may also have artificially lowered our findings of gray-scale sensitivity to tumor in individual segments. In addition, all of our patients had diffuse bilateral disease, which may account in part for the paucity of focal lesions detectable at US (8). False-negative findings at sonoelasticity imaging may have resulted from small amounts of tumor in the imaged segment, infiltrative tumor without enough fibrosis or stiffening to cause a change in vibration, or mismatch of imaging segments with pathologic sections, because our study protocol did not permit precise correlation but only a regional estimate of tumor presence or absence.

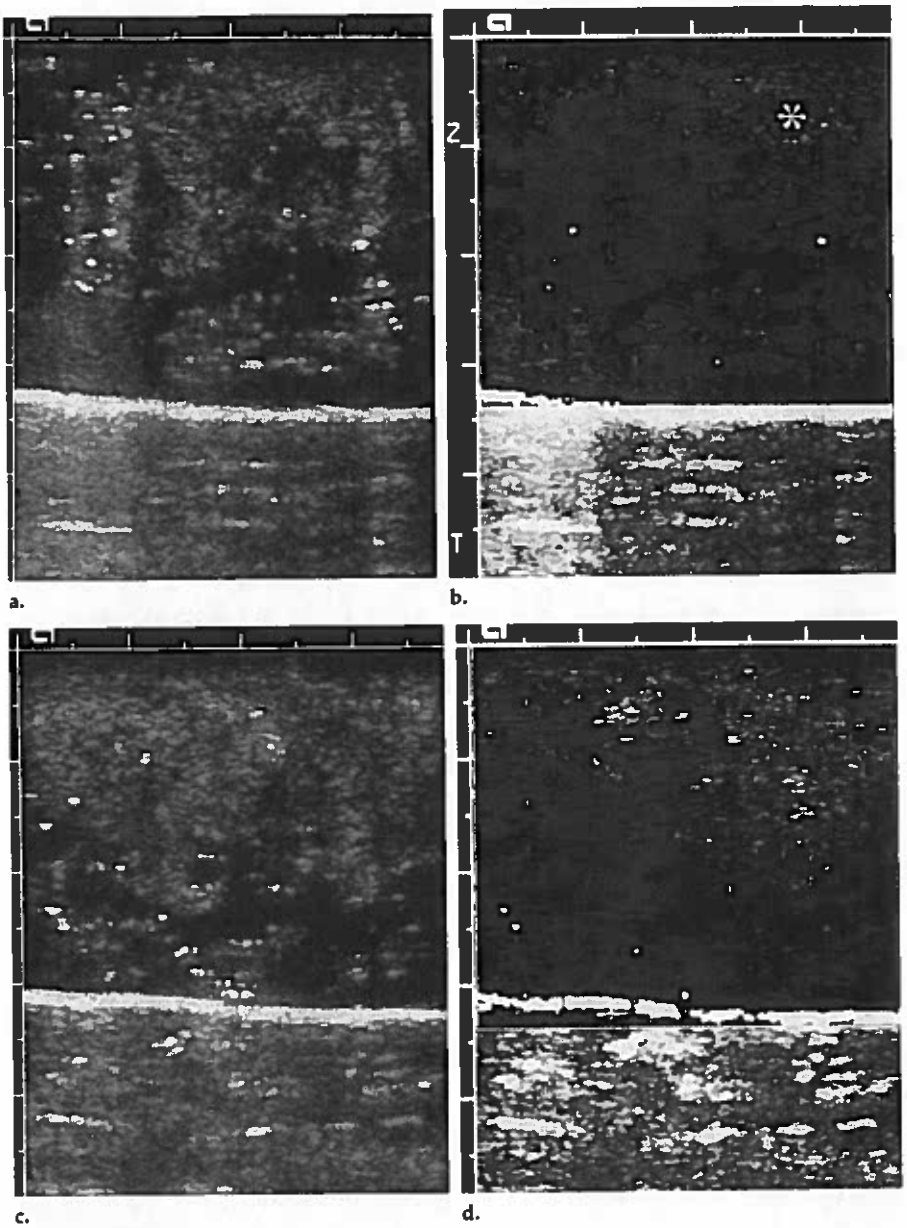

Figure 4. Diffuse carcinoma demonstrated at multiple frequencies in a 69-year-old man with no palpable abnormality and a serum PSA level of 6.7 ng/mL. **(a)** Standard prone transverse US image obtained at the base of the prostate demonstrates somewhat heterogeneous echotexture. **(b)** Corresponding sonoelasticity image obtained at 50 Hz shows poor vibration diffusely, most pronounced posteriorly on the right (*). **(c)** A second section of the base, obtained slightly caudal to **a**, shows a heterogeneous gray-scale pattern. **(d)** Corresponding sonoelasticity image obtained at 150 Hz documents absent bilateral posterior and right anterior vibration.

Hypoechoic lesions detected at transrectal US show low specificity for carcinoma unless accompanied by other indicators of carcinoma such as positive results of digital rectal examination or elevated PSA levels (10–12). Thus, sonoelasticity imaging has potential to improve the specificity of standard transrectal US biopsy by avoidance of sampling of hypoechoic regions at standard US that demonstrate a normal vibration pattern at sonoelasticity imaging. In the current study, false-positive results at sonoelasticity imaging included prostatic intraepithelial neoplasia, and stromal hyperplasia with 8–10-mm nodules that may have been stiff enough and large enough to disrupt the vibration pattern in two cases. Dense diffuse stromal hyperplasia also may have displaced enough glandular tissue to diminish vibration.

Some variation in sonoelasticity imaging results was noted between

readers. The sensitivity of sonoelasticity imaging with both readers, however, was far superior to that of gray-scale US in individual segments. Readers agreed on more than 80% of image interpretations; interobserver agreement with the κ statistic, however, was low. This was due in part to asymmetry of the sample, in which more than 60% of readings were positive because of the large number of tumor-containing segments present. This diminished the opportunity for observer disagreement, and the κ statistic was, therefore, based on a smaller chance group. In addition, sonoelasticity imaging is a new technique, and image interpretation is subjective.

Our results are preliminary because the vibration equipment is prototypical and the receiver-imaging aspects of sonoelasticity imaging have yet to be optimized and standardized, along with optimization of the vibration source and frequency. The relatively poor detection of tumor in the anterior segments raises the possibility of tissue saturation in proximity to the vibration source. These findings will require further investigation. In vivo application will require an adequate patient vibration source and receiver programs for use with endocavitary transducers. Then, with a mixed population with benign and malignant pathologic conditions, in vivo results must corroborate our in vitro experience before sonoelasticity imaging can be adapted for clinical use. ■

Acknowledgments: The authors thank Acuson Corporation for generous technical support in the development of this project and Beverly Pollet and Margaret Kowaluk for manuscript preparation.

References

1. Lerner RM, Huang SR, Parker KJ. "Sonoelasticity" images derived from ultrasound signals in mechanically vibrated tissues. Ultrasound Med Biol 1990; 16:231–239.
2. Lee F Jr, Bronson JP, Lerner RM, Parker KJ, Huang SR, Roach DJ. Sonoelasticity imaging: results in in vitro tissue specimens. Radiology 1991; 181:237–239.
3. Dähnert WI, Hamper UM, Eggleston JC, Walsh PC, Sanders RC. Prostatic evaluation by transrectal sonography with histopathologic correlation: the echopenic appearance of early carcinoma. Radiology 1986; 158:97–102.
4. Lee F, Gray JM, McLeary RD, et al. Prostatic evaluation by transrectal sonography: criteria for diagnosis of early carcinoma. Radiology 1986; 158:91–95.
5. Dyke CH, Toi A, Sweet JM. Value of random US-guided transrectal prostate biopsy. Radiology 1990; 176:345–349.
6. Fleiss JL. The measurement of interrator agreement. In: Statistical methods for rates and proportions. New York, NY: Wiley, 1981, 212ff.
7. Coffield KS, Speights VO, Brawn PN, Riggs MW. Ultrasound detection of prostate cancer in postmortem specimens with histological correlation. J Urol 1992; 147:822–826.
8. Slonim SM, Cuttino JT Jr, Johnson CJ, et al. Diagnosis of prostatic carcinoma: value of random transrectal sonographically guided biopsies. AJR 1993; 161:1003–1006.
9. Daniels GF Jr, McNeal JE, Stamey TA. Predictive value of contralateral biopsies in unilaterally palpable prostate cancer. J Urol 1992; 147:870–874.
10. Billebaud T, Villers A, Astier L, et al. Advantage of systematic random ultrasound-guided biopsies: measurement of serum prostate-specific antigen level and determination of prostate volume in the early diagnosis of prostate cancer. Eur Urol 1992; 21: 6–14.
11. Lee F, Torp-Pedersen S, Littrup PJ, et al. Hypoechoic lesions of the prostate: clinical relevance of tumor size, digital rectal examination, and prostate-specific antigen. Radiology 1989; 170:29–32.
12. Hodge KK, McNeal JE, Stamey TA. Ultrasound guided transrectal core biopsies of the palpably abnormal prostate. J Urol 1989; 142:66–70.